# Absorption switches in metal-dielectric-metal plasmonic waveguides

**Changjun Min[1] and Georgios Veronis[1,2]**

[1]*Center for Computation and Technology, Louisiana State University, Baton Rouge, Louisiana 70803*
[2]*Department of Electrical and Computer Engineering, Louisiana State University, Baton Rouge, Louisiana 70803*
*gveronis@lsu.edu*

**Abstract:** We theoretically investigate the properties of absorption switches for metal-dielectric-metal (MDM) plasmonic waveguides. We show that a MDM waveguide directly coupled to a cavity filled with an active material with tunable absorption coefficient can act as an absorption switch, in which the on/off states correspond to the absence/presence of optical pumping. We also show that a MDM plasmonic waveguide side-coupled to a cavity filled with an active material can operate as an absorption switch, in which the on/off states correspond to the presence/absence of pumping. For a specific modulation depth, the side-coupled-cavity switch results in more compact designs compared to the direct-coupled-cavity switch. Variations in the imaginary part of the refractive index of the material filling the cavity of $\Delta\kappa = 0.01$ ($\Delta\kappa = 0.15$) result in ~60% (~99%) modulation depth. The properties of both switches can be accurately described using transmission line theory.



**OCIS codes:** (130.2790) Guided waves; (240.6680) Surface Plasmons; (130.4815) Optical switching devices.

## References and links

1. W. L. Barnes, A. Dereux, and T. W. Ebbesen, "Surface plasmon subwavelength optics," Nature **424**(6950), 824–830 (2003).
2. E. Ozbay, "Plasmonics: merging photonics and electronics at nanoscale dimensions," Science **311**(5758), 189–193 (2006).
3. R. Zia, J. A. Schuller, A. Chandran, and M. L. Brongersma, "Plasmonics: the next chip-scale technology," Mater. Today **9**(7-8), 20–27 (2006).
4. S. A. Maier, *Plasmonics: fundamentals and applications*, (Springer, New York, 2007).
5. H. A. Atwater, "The promise of plasmonics," Sci. Am. **296**(4), 56–63 (2007).
6. A. V. Krasavin, and N. I. Zheludev, "Active plasmonics: Controlling signals in Au/Ga waveguide using nanoscale structural transformations," Appl. Phys. Lett. **84**(8), 1416–1418 (2004).
7. T. Nikolajsen, K. Leosson, and S. I. Bozhevolnyi, "Surface plasmon polariton based modulators and switches operating at telecom wavelengths," Appl. Phys. Lett. **85**(24), 5833–5835 (2004).
8. A. L. Lereu, A. Passian, J.-P. Goudonnet, T. Thundat, and T. L. Ferrell, "Optical modulation processes in thin films based on thermal effects of surface plasmons," Appl. Phys. Lett. **86**(15), 154101 (2005).
9. K. F. MacDonald, Z. L. Sámson, M. I. Stockman, and N. I. Zheludev, "Ultrafast active plasmonics," Nat. Photonics **3**(1), 55–58 (2009).
10. G. A. Wurtz, and A. V. Zayats, "Nonlinear surface plasmon polaritonic crystals," Laser Photon. Rev. **2**(3), 125–135 (2008).
11. C. Min, P. Wang, C. Chen, Y. Deng, Y. Lu, H. Ming, T. Ning, Y. Zhou, and G. Yang, "All-optical switching in subwavelength metallic grating structure containing nonlinear optical materials," Opt. Lett. **33**(8), 869–871 (2008).
12. M. J. Dicken, L. A. Sweatlock, D. Pacifici, H. J. Lezec, K. Bhattacharya, and H. A. Atwater, "Electrooptic Modulation in Thin Film Barium Titanate Plasmonic Interferometers," Nano Lett. **8**(11), 4058–4052 (2008).
13. W. Dickson, G. A. Wurtz, P. R. Evans, R. J. Pollard, and A. V. Zayats, "Electronically controlled surface plasmon dispersion and optical transmission through metallic hole arrays using liquid crystal," Nano Lett. **8**(1), 281–286 (2008).
14. Z. Yu, G. Veronis, S. Fan, and M. L. Brongersma, "Gain-induced switching in metal-dielectric-metal plasmonic waveguides," Appl. Phys. Lett. **92**(4), 041117 (2008).
15. R. A. Pala, K. T. Shimizu, N. A. Melosh, and M. L. Brongersma, "A nonvolatile plasmonic switch employing photochromic molecules," Nano Lett. **8**(5), 1506–1510 (2008).
16. D. Pacifici, H. J. Lezec, and H. A. Atwater, "All-optical modulation by plasmonic excitation of CdSe quantum dots," Nat. Photonics **1**(7), 402–406 (2007).
17. D. Pacifici, H. J. Lezec, L. A. Sweatlock, C. D. Ruiter, V. Ferry, and H. A. Atwater, "All-optical plasmonic

#111340 - $15.00 USD Received 13 May 2009; revised 7 Jun 2009; accepted 8 Jun 2009; published 11 Jun 2009

modulators and interconnects," in *Plasmonic nanoguides and circuits*, S. I. Bozhevolnyi, ed. (World Scientific, 2009).
18. J. R. Krenn, B. Lamprecht, H. Ditlbacher, G. Schider, M. Salerno, A. Leitner, and F. R. Aussenegg, "Non-diffraction-limited light transport by gold nanowires," Europhys. Lett. **60**(5), 663–669 (2002).
19. S. A. Maier, P. G. Kik, H. A. Atwater, S. Meltzer, E. Harel, B. E. Koel, and A. A. G. Requicha, "Local detection of electromagnetic energy transport below the diffraction limit in metal nanoparticle plasmon waveguides," Nat. Mater. **2**(4), 229–232 (2003).
20. S. I. Bozhevolnyi, V. S. Volkov, E. Devaux, J. Y. Laluet, and T. W. Ebbesen, "Channel plasmon subwavelength waveguide components including interferometers and ring resonators," Nature **440**(7083), 508–511 (2006).
21. R. Zia, M. D. Selker, P. B. Catrysse, and M. L. Brongersma, "Geometries and materials for subwavelength surface plasmon modes," J. Opt. Soc. Am. A **21**(12), 2442–2446 (2004).
22. G. Veronis, and S. Fan, "Bends and splitters in subwavelength metal-dielectric-metal plasmonic waveguides," Appl. Phys. Lett. **87**, 131102 (2005).
23. A. Hosseini, and Y. Massoud, "Nanoscale surface plasmon based resonator using rectangular geometry," Appl. Phys. Lett. **90**(18), 181102 (2007).
24. Y. Matsuzaki, T. Okamoto, M. Haraguchi, M. Fukui, and M. Nakagaki, "Characteristics of gap plasmon waveguide with stub structures," Opt. Express **16**(21), 16314–16325 (2008).
25. X. S. Lin, and X. G. Huang, "Tooth-shaped plasmonic waveguide filters with nanometeric sizes," Opt. Lett. **33**(23), 2874–2876 (2008).
26. D. M. Pozar, *Microwave Engineering*, (Wiley, New York, 1998).
27. E. N. Economou, "Surface plasmons in thin films," Phys. Rev. **182**(2), 539–554 (1969).
28. G. Veronis, and S. Fan, "Overview of Simulation Techniques for Plasmonic Devices," in *Surface Plasmon Nanophotonics*, Mark L. Brongersma and Pieter G. Kik, ed. (Springer, 2007).
29. E. D. Palik, *Handbook of Optical Constants of Solids*, (Academic, New York, 1985).
30. J. Jin, *The Finite Element Method in Electromagnetics*, (Wiley, New York, 2002).
31. S. Ramo, J. R. Whinnery, and T. Van Duzer, *Fields and Waves in Communication Electronics*, (Wiley, New York, 1994).
32. H. A. Haus, and Y. Lai, "Narrow-band distributed feedback reflector design," IEEE J. Lightwave Technol. **9**(6), 754–760 (1991).
33. H. A. Haus, and Y. Lai, "Theory of Cascaded Quarter Wave Shifted Distributed Feedback Resonators," IEEE J. Quantum Electron. **28**(1), 205–213 (1992).
34. D. Pacifici, H. J. Lezec, H. A. Atwater, and J. Weiner, "Quantitative determination of optical transmission through subwavelength slit arrays in Ag films: Role of surface wave interference and local coupling between adjacent slits," Phys. Rev. B **77**(11), 115411 (2008).
35. D. Pacifici, H. J. Lezec, L. A. Sweatlock, R. J. Walters, and H. A. Atwater, "Universal optical transmission features in periodic and quasiperiodic hole arrays," Opt. Express **16**(12), 9222–9238 (2008).
36. S. E. Kocabas, G. Veronis, D. A. B. Miller, and S. Fan, "Transmission line and equivalent circuit models for plasmonic waveguide components," IEEE J. Sel. Top. Quantum Electron. **14**(6), 1462–1472 (2008).
37. J. Liu, M. Beals, A. Pomerene, S. Bernardis, R. Sun, J. Cheng, L. C. Kimerling, and J. Michel, "Waveguide-integrated, ultralow-energy GeSi electro-absorption modulators," Nat. Photonics **2**(7), 433–437 (2008).
38. Q. Xu, S. Manipatruni, B. Schmidt, J. Shakya, and M. Lipson, "12.5 Gbit/s carrier-injection-based silicon micro-ring silicon modulators," Opt. Express **15**, 430–436 (2007).
39. I. Bar-Joseph, C. Klingshirn, D. A. B. Miller, D. S. Chemla, U. Koren, and B. I. Miller, "Quantum-confined Stark effect in InGaAs/InP quantum wells grown by organometallic vapor phase epitaxy," Appl. Phys. Lett. **50**(15), 1010 (1987).
40. S. Sandhu, M. L. Povinelli, and S. Fan, "Stopping and time reversing a light pulse using dynamic loss tuning of coupled-resonator delay lines," Opt. Lett. **32**(22), 3333–3335 (2007).

## 1. Introduction

Plasmonic devices, based on surface plasmons propagating at metal-dielectric interfaces, have shown the potential to guide and manipulate light at deep subwavelength scales [1–5]. One of the main challenges in plasmonics is achieving active control of optical signals in nanoscale plasmonic devices [2]. This challenge has motivated significant recent activities in exploring actively-controlled plasmonic devices, such as switches and modulators [6–17]. Several different approaches have been proposed in order to achieve active control of light in nanoscale plasmonic devices [6–17]. These include thermally-induced changes in the refractive index [6–8], direct ultrafast optical excitation of the metal [9], as well as the incorporation of nonlinear [10,11], electrooptic [12,13], and gain [14] media in plasmonic devices. An alternative approach for active control of optical signals in plasmonic devices is tuning the absorption coefficient. This has been recently achieved experimentally through optical excitation of photochromic molecules [15] or CdSe quantum dots (QDs) [16,17].

In this paper, we investigate absorption switches for metal-dielectric-metal (MDM) plasmonic waveguides. Several different nanoscale plasmonic waveguiding structures have

#111340 - $15.00 USD Received 13 May 2009; revised 7 Jun 2009; accepted 8 Jun 2009; published 11 Jun 2009

been recently proposed, such as metallic nanowires, metallic nanoparticle arrays, V-shaped grooves, and MDM waveguides [18–25]. Among these, MDM plasmonic waveguides, which are the optical analogue of microwave two-conductor transmission lines [26], are of particular interest because they support modes with deep subwavelength scale and high group velocity over a very wide range of frequencies extending from DC to visible [27]. Thus, MDM waveguides could be potentially important in providing an interface between conventional optics and subwavelength electronic and optoelectronic devices.

Here we first consider a switch consisting of a MDM plasmonic waveguide directly coupled to a cavity filled with an active material whose absorption coefficient can be modified with an external control beam. We show that such a direct-coupled-cavity structure can act as an absorption switch, in which the on/off states correspond to the absence/presence of pumping. We also consider a switch consisting of a MDM plasmonic waveguide side-coupled to a cavity filled with an active material. We show that the side-coupled structure can also operate as an absorption switch, in which the on/off states correspond to the presence/absence of optical pumping. For a specific modulation depth, the side-coupled-cavity switch results in more compact designs, when compared with the direct-coupled-cavity switch. Variations in the imaginary part of the refractive index of the material filling the cavity of $\Delta\kappa = 0.01$ ($\Delta\kappa = 0.15$) result in ~60% (~99%) modulation depth. In addition, the operation wavelength range of the switch is broad. Finally, the properties of both switches can be accurately described using the concept of characteristic impedance and transmission line theory.

The side-coupled-cavity structures, consisting of a rectangular cavity connected in series to a MDM waveguide, are analogous to the stub resonators used in impedance matching networks and microwave filters [26]. In previous studies, such side-coupled-cavity structures have been proposed as compact filters and impedance matching elements for plasmonic waveguides [24,25].

The remainder of the paper is organized as follows. In Section 2, we first briefly describe the simulation method used for the analysis of the switch structures. The results obtained for the direct-coupled-cavity and side-coupled-cavity switch structures are presented in Subsections 2.1 and 2.2, respectively. Finally, our conclusions are summarized in Section 3.

## 2. Results

We use a two-dimensional finite-difference frequency-domain (FDFD) method [28] to calculate the transmission of the absorption switches. This method allows us to directly use experimental data for the frequency-dependent dielectric constant of metals such as silver [29], including both the real and imaginary parts, with no approximation. Perfectly matched layer (PML) absorbing boundary conditions are used at all boundaries of the simulation domain [30]. In all cases considered the widths of the MDM plasmonic waveguides are much smaller than the wavelength, so that only the fundamental transverse magnetic (TM) waveguide mode is propagating.

### *2.1 Direct-coupled-cavity switch*

We first consider a switch consisting of a silver-air-silver MDM plasmonic waveguide directly coupled to a cavity (Fig. 1(a)). The cavity is filled with a material with refractive index $n = 2.02 + i\kappa$, corresponding to CdSe QD-doped silicon dioxide [17]. The imaginary part $\kappa$ of the refractive index can be modified with an external control (pump) beam. In the absence of pumping, the QD-doped material is transparent to infrared photons, since their energy is smaller than the QD bandgap. In contrast, in the presence of pumping, infrared photons are absorbed by an intraband transition in the QDs which are excited by the pump beam [16,17]. We consider experimentally achievable values of $\kappa$ in the range $0<\kappa<1$ [17]. (In Ref [17], the refractive index of CdSe QD-doped silicon dioxide was directly measured by spectroscopic ellipsometry). Such high absorption coefficient is enabled by the large absorption cross section of CdSe QDs [16,17]. In Fig. 1(b) (Fig. 1(c)) we show the transmission of such a direct-coupled-cavity switch as a function of the length $L$ of the cavity in the absence (presence) of optical pumping. In the absence of pumping (Fig. 1(b)), the

#111340 - $15.00 USD Received 13 May 2009; revised 7 Jun 2009; accepted 8 Jun 2009; published 11 Jun 2009

material filling the cavity is in its transparent state ($\kappa = 0$), and the transmission of the structure as a function of the cavity length $L$ exhibits typical Fabry-Perot oscillations. We observe that at the Fabry-Perot resonant peaks, there is almost complete transmission of the incident optical mode. In contrast, in the presence of pumping (Fig. 1(c)), the material filling the cavity is in its absorbing state ($\kappa = 1$), and the transmission of the switch decreases roughly exponentially with the cavity length $L$. If $L$ is long enough, the incident optical mode is almost completely absorbed in the cavity, and there is almost no transmission. Thus, we observe that such a direct-coupled-cavity structure can act as an absorption switch for MDM plasmonic waveguides, in which the on/off states correspond to the absence/presence of pumping.

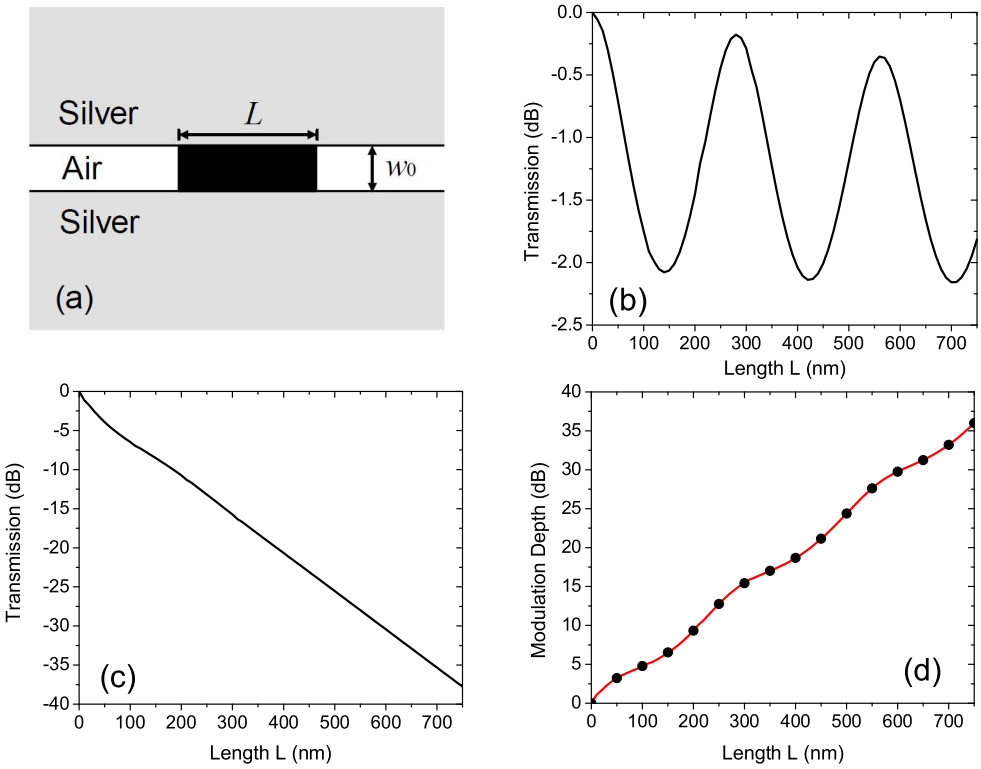


Fig. 1. (a) Schematic of a switch consisting of a silver-air-silver MDM plasmonic waveguide directly coupled to a cavity filled with a material with refractive index $n = 2.02 + i\kappa$. The imaginary part $\kappa$ of the refractive index can be modified with an external control beam. (b) Transmission of the switch as a function of the length $L$ of the cavity at $\lambda_0 = 1.55\mu m$ in the absence of pumping ($\kappa = 0$) calculated using FDFD. Results are shown for $w_0 = 50nm$. (c) Same as (b), except that there is pumping of the material filling the cavity ($\kappa = 1$). (d) Modulation depth of the switch $T(\kappa = 0)/T(\kappa = 1)$ as a function of $L$ calculated using FDFD (dots). We also show the modulation depth calculated using transmission line theory (solid line). All other parameters are as in (b).

In Fig. 1(d) we show the modulation depth of the switch (defined as the ratio of the transmission in the *on* state to the transmission in the *off* state $T(\kappa = 0)/T(\kappa = 1)$) as a function of the cavity length $L$ at $\lambda_0 = 1.55\mu m$. We observe that the modulation depth increases with the cavity length $L$. The increase is almost exponential with slight oscillations associated with the Fabry-Perot response in the *on* state. We also found that the modulation depth can be further increased by decreasing the width of the cavity.

The properties of systems such as the direct-coupled-cavity switch (Fig. 1(a)), which consist of circuits of deep subwavelength MDM plasmonic waveguides, can be described using the concept of characteristic impedance and transmission line theory [22,26,31]. Based on transmission line theory, the direct-coupled-cavity switch is equivalent to a transmission

#111340 - $15.00 USD Received 13 May 2009; revised 7 Jun 2009; accepted 8 Jun 2009; published 11 Jun 2009

line segment of length $L$ and characteristic impedance $Z_2$, which is sandwiched between two semi-infinite transmission lines with characteristic impedance $Z_1$. The characteristic impedances $Z_i$ are given by [22]

$$Z_i = \frac{\gamma_i}{j\omega\varepsilon_i} w_i, \; i = 1,2 \tag{1}$$

where ω is the frequency, $j = \sqrt{-1}$, $\varepsilon_i$ and $w_i$ are the dielectric permittivity and width, respectively, of the dielectric region of the MDM waveguide, and $\gamma_i$ is the complex propagation constant of the fundamental propagating TM mode in the MDM waveguide. Thus, for the switch of Fig. 1(a) we have $\varepsilon_1 = \varepsilon_0$, $\varepsilon_2 = n^2\varepsilon_0$, and $w_1 = w_2 = w_0$. Based on transmission line theory [26], the transmission $T$ of the direct-coupled-cavity switch can be calculated as

$$T = \left| \cosh(\gamma_2 L) + \frac{1}{2}\left( \frac{Z_1}{Z_2} + \frac{Z_2}{Z_1} \right) \sinh(\gamma_2 L) \right|^{-2}. \tag{2}$$

In Fig. 1(d) we show the modulation depth of the switch calculated by transmission line theory. We observe that there is excellent agreement between the transmission line theory results and the exact results obtained using FDFD. This agreement suggests that the concept of characteristic impedance and transmission line theory are indeed valid and useful to describe the properties of the switch.

*2.2 Side-coupled-cavity switch*

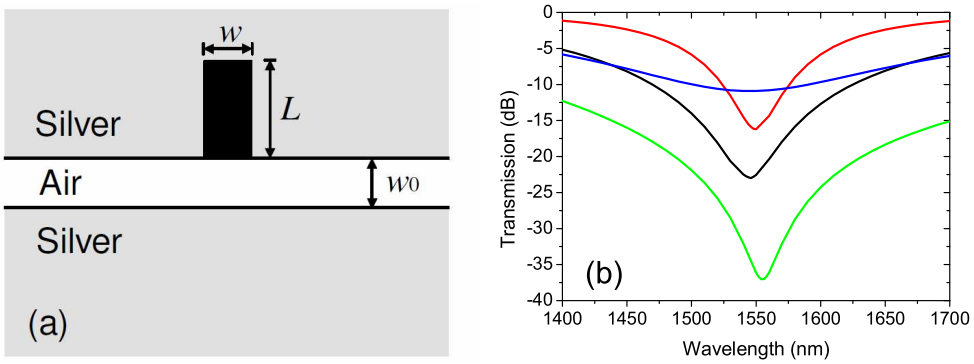


Fig. 2. (a) Schematic of a switch consisting of a silver-air-silver MDM plasmonic waveguide side-coupled to a cavity filled with an absorbing material as in Fig. 1(a). (b) Transmission spectra of the switch calculated using FDFD. Results are shown for $w$ = 50nm, $L$ = 120nm, $\kappa$ = 0 (black curve), $w$ = 50nm, $L$ = 405nm, $\kappa$ = 0 (red curve), $w$ = 200nm, $L$ = 175nm, $\kappa$ = 0 (green curve), and $w$ = 50nm, $L$ = 120nm, $\kappa$ = 0.1 (blue curve). All other parameters are as in Fig. 1(b).

We now consider a switch consisting of a silver-air-silver MDM plasmonic waveguide side-coupled to a cavity filled with a material with tunable absorption coefficient ($n$ = 2.02 + i$\kappa$) (Fig. 2(a)). The properties of such a side-coupled-cavity switch can also be described using transmission line theory and the concept of characteristic impedance. Based on transmission line theory, the side-coupled-cavity switch is equivalent to a short-circuited transmission line resonator of length $L$, propagation constant $\gamma_2$, and characteristic impedance $Z_2$, which is connected in series to a transmission line with characteristic impedance $Z_1$ [26]. Based on this model, the transmission $T$ of the side-coupled-cavity switch can be calculated using transmission line theory [26] as

#111340 - $15.00 USD Received 13 May 2009; revised 7 Jun 2009; accepted 8 Jun 2009; published 11 Jun 2009

$$T = \left| 1 + \frac{Z_2}{2Z_1} \tanh(\gamma_2 L) \right|^{-2} \tag{3}$$

As seen from Eq. (3), the system exhibits a resonance when $\beta_2 L = (N + 1/2)\pi$, where $\gamma_2 = \alpha_2 + j\beta_2$, and $N$ is an integer. We assume that the cavity length $L$ is equal to one of the resonant lengths $L_N$ at frequency $\omega_0$, and consider the response of the system for frequencies $\omega$ in the vicinity of $\omega_0$ ($\frac{|\omega - \omega_0|}{\omega_0} << 1$) . In such a case, we find that Eq. (3) can be approximated as

$$T(\omega) \simeq \frac{(\omega - \omega_0)^2 + \left(\frac{\omega_0}{2Q_0}\right)^2}{(\omega - \omega_0)^2 + \left(\frac{\omega_0}{2Q_0} + \frac{\omega_0}{2Q_e}\right)^2}, \tag{4}$$

where

$$Q_0 = \frac{\omega_0}{2\alpha_2 v_g}, Q_e = \frac{Z_1}{Z_2}\frac{\omega_0 L_N}{v_g}, \tag{5}$$

and $v_g = \frac{\partial \omega}{\partial \beta_2}$. Here $Q_0$ is the quality factor associated with the internal loss in the cavity due to the propagation loss of the optical mode, and $Q_e$ is the quality factor associated with the power escape through the waveguide. We note that Eq. (4) can also be directly derived using coupled-mode theory and first-principles calculation of the quality factors $Q_0$ and $Q_e$ [32,33]. We observe that the on-resonance transmission is a function of the ratio $r$ of the quality factors, i.e.

$$T(\omega_0) \simeq \left(\frac{r}{r+1}\right)^2, \; r = \frac{Q_e}{Q_0} = \frac{Z_1}{Z_2} 2\alpha_2 L_N \tag{6}$$

Since both $\alpha_2$ and $Z_2$ depend on the imaginary part $\kappa$ of the refractive index in the cavity, the transmission of the system can be controlled by modifying $\kappa$ with an external beam.

In Fig. 2(b) we show the transmission spectra of the side-coupled-cavity structure for $w = w_0 = 50$nm in the absence of optical pumping ($\kappa = 0$) calculated using FDFD. The length of the cavity $L$ is chosen $L = 120$nm, so that the system exhibits a resonance at $\lambda_0 = 1.55\mu$m. The transmission spectra are characterized by a Lorentzian lineshape, as predicted by Eq. (4). We observe that, as $|\omega-\omega_0|$ increases, the transmission increases, and, in the limit $|\omega-\omega_0|\to\infty$, the transmission approaches 1 ($\lim_{|\omega-\omega_0|\to\infty} T(\omega) = 1$). In other words, if $\omega$ is far from the resonant frequency $\omega_0$, the incident waveguide mode is almost completely transmitted. At resonance ($\omega = \omega_0$), we observe that the transmission is less than 1% ($T(\omega_0)\approx$-23dB). When the material filling the cavity is in its transparent state ($\kappa = 0$), the propagation loss of the optical mode is only associated with the loss in the metal. In that case, the propagation length is in the order of tens of micrometers at near-infrared wavelengths [21], so that $\alpha_2 L << 1$, and therefore $r << 1$ and $T << 1$ (Eq. (6)). In addition, since $r << 1$, the total quality factor, defined as $Q \equiv (Q_0^{-1} + Q_e^{-1})^{-1}$, is $Q \simeq Q_e \simeq 4.4$ (Eq. (5)), and the system response is broad (Fig. 2(b)). The low quality factor in this structure is associated with the low reflectivity at the waveguide-cavity interface due to the small impedance mismatch.

If the stub length $L$ increases to the second resonant length ($L = 405$nm is chosen as before so that the system exhibits a resonance at $\lambda_0 = 1.55\mu$m), more energy is stored in the resonant

#111340 - $15.00 USD Received 13 May 2009; revised 7 Jun 2009; accepted 8 Jun 2009; published 11 Jun 2009

cavity, so that $Q_e$ increases (Eq. (5)), and therefore the on resonance transmission also increases (Eq. (6)). We indeed observe that for $L$ = 405nm the transmission is higher than for $L$ = 120nm in the entire frequency range (Fig. 2(b)).

If the stub width $w$ increases ($w$ = 200nm, and $L$ = 175nm is chosen as before so that the system exhibits a resonance at $\lambda_0$ = 1.55μm), the propagation length of the optical mode in the cavity increases, leading to higher $Q_0$ (Eq. (5)). In addition, the wider $w$ leads to larger power escape through the waveguide, and therefore lower $Q_e$. Hence the on resonance transmission decreases (Eq. (6)). We indeed observe that for wider $w$ the transmission is lower in the entire frequency range (Fig. 2(b)).

In the presence of optical pumping, the material in the stub switches to its absorbing state. The internal loss in the cavity increases, and therefore $Q_0$ decreases, resulting in higher on-resonance transmission (Eq. (6)). We indeed observe that for $\kappa$ = 0.1 the on resonance transmission is significantly larger than for $\kappa$ = 0 (Fig. 2(b)). Thus, the side-coupled structure can also operate as an absorption switch for MDM plasmonic waveguides, in which the on/off states correspond to the presence/absence of optical pumping.

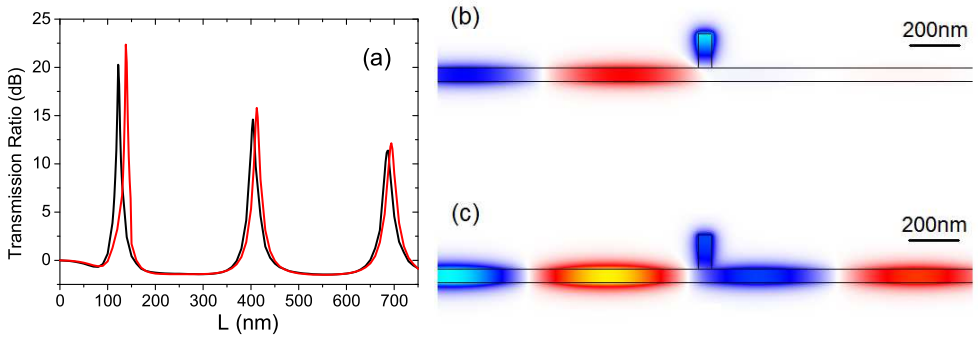


Fig. 3. (a) Modulation depth $T(\kappa = 1)/T(\kappa = 0)$ of the side-coupled-cavity switch (Fig. 2(a)) as a function of the stub length $L$ calculated using FDFD (black curve), and transmission line theory (red curve). Results are shown for $w$ = 50nm. All other parameters are as in Fig. 2(b). (b) Magnetic field profile of the switch for $L$ = 120nm in the absence of pumping ($\kappa$ = 0). All other parameters are as in (a). (c) Magnetic field profile of the switch in the presence of pumping ($\kappa$ = 1). All other parameters are as in (b).

In Fig. 3(a) we show the modulation depth of the switch $T(\kappa = 1)/T(\kappa = 0)$ as a function of the cavity length $L$ at $\lambda_0$ = 1.55μm calculated with FDFD. We observe that the modulation depth exhibits peaks when $L$ is equal to one of the resonant lengths of the stub. This is due to the fact that the transmission in the absence of pumping $T(\kappa = 0)$ is minimized on resonance, as described above. We also observe that the maximum modulation depth is obtained when the cavity length $L$ is equal to the first resonant length. As described above, if the stub length $L$ increases to a higher-order resonant length, the quality factor $Q_e$ increases and leads to larger on resonance transmission. This occurs both in the presence and in the absence of pumping, i.e. both $T(\kappa = 1)$ and $T(\kappa = 0)$ increase. In the absence of pumping ($\kappa$ = 0), we have $r \ll 1$ for the ratio $r$ of the quality factors, as mentioned above. Thus, based on Eq. (6), the on resonance transmission in the absence of pumping varies roughly quadratically with $r$. On the other hand, in the presence of pumping, $r$ is much larger, and the on resonance transmission is, therefore, less sensitive to $r$ (Eq. (6)). In other words, if the stub length $L$ increases to a higher-order resonant length, the on resonance transmission in the absence of pumping $T(\kappa = 0)$ increases more than the on resonance transmission in the presence of pumping $T(\kappa = 1)$. Thus, the modulation depth $T(\kappa = 1)/T(\kappa = 0)$ decreases (Fig. 3(a)). In Fig. 3(a) we also show the modulation depth of the switch calculated by transmission line theory (Eq. (3)). We again observe that there is very good agreement between the transmission line theory results and the exact results obtained using FDFD, verifying the validity and usefulness of the transmission line theory model for the side-coupled-cavity switch of Fig. 2(a). We note that the small difference between the transmission line theory results and the exact results obtained using

#111340 - $15.00 USD Received 13 May 2009; revised 7 Jun 2009; accepted 8 Jun 2009; published 11 Jun 2009

FDFD is due to the error introduced by the transmission line model in the phase of the reflection coefficient [34,35] at the two interfaces of the side-coupled cavity of length $L$. Such limitations of the transmission line model for circuits of MDM plasmonic waveguides have been described in detail elsewhere [36].

In Figs. 3(b) and (c) we show the magnetic field profile of the side-coupled-cavity switch corresponding to the *off* and *on* states, respectively. In the absence of pumping, corresponding to the *off* state, the incident optical mode is almost completely reflected. In contrast, in the presence of pumping, corresponding to the *on* state, the transmission increases by more than two orders of magnitude leading to a large modulation depth.

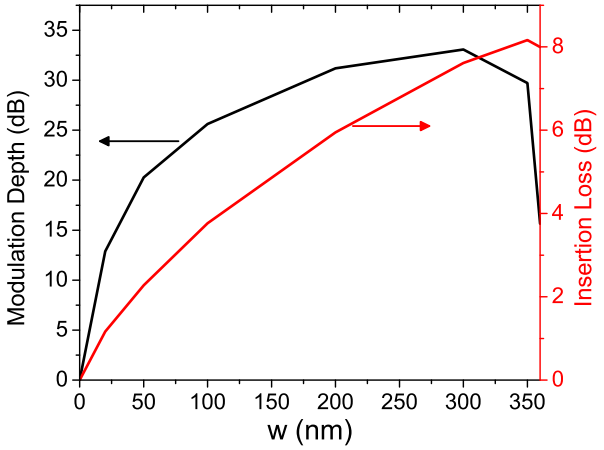


Fig. 4. Modulation depth $T(\kappa = 1)/T(\kappa = 0)$ (black curve) and insertion loss (red curve) of the side-coupled-cavity switch (Fig. 2(a)) as a function of the stub width $w$. For each stub width $w$, the stub length $L$ is equal to the first resonant length of the cavity. All other parameters are as in Fig. 2(b).

In Fig. 4 we show the maximum modulation depth of the side-coupled-cavity switch as a function of the stub width $w$. As mentioned above, for a given $w$ the maximum modulation depth is achieved when the stub length $L$ is equal to the first resonant length. We observe that for $w$<300nm the maximum modulation depth increases with $w$. As described above, larger $w$ leads to both higher $Q_0$ and lower $Q_e$ for the resonator. Thus, the quality factors ratio $r$ decreases, and the on resonance transmission decreases (Eq. (6)). This occurs both in the presence and in the absence of pumping, i.e. both $T(\kappa = 1)$ and $T(\kappa = 0)$ decrease. However, as mentioned above, in the absence of pumping ($\kappa = 0$) the on resonance transmission is more sensitive to $r$. Thus, as the stub width $w$ increases, the on resonance transmission in the absence of pumping $T(\kappa = 0)$ decreases more than the on resonance transmission in the presence of pumping $T(\kappa = 1)$. Thus, the modulation depth $T(\kappa = 1)/T(\kappa = 0)$ increases with $w$ (Fig. 4). We also observe that the modulation depth is maximized for $w \simeq 300\text{nm}$. In other words, for a given pumping intensity there is a maximum achievable modulation depth for the side-coupled-cavity structure. We found that the decrease with $w$ of the modulation depth for $w$>300nm is associated with the excitation of higher order modes in the resonator, which occurs when $w$ becomes comparable to the wavelength. In this regime, the transmission line model breaks down, and the system properties are no longer accurately described by Eqs. (3)-(6).

In Fig. 4 we also show the insertion loss of the side-coupled-cavity switch, defined as $-10\log_{10}(T(\kappa = 1))$, as a function of the stub width $w$. As described above, for $w$<300nm the on resonance transmission in the presence of pumping $T(\kappa = 1)$ decreases with $w$, and the insertion loss therefore increases (Fig. 4). For $w$>300nm, the insertion loss decreases with $w$ (Fig. 4), due to the excitation of higher order modes in the resonator, as also described above. We observe that for the side-coupled-cavity switch there is a trade off between modulation

#111340 - $15.00 USD Received 13 May 2009; revised 7 Jun 2009; accepted 8 Jun 2009; published 11 Jun 2009

depth and insertion loss, as the geometrical parameters of the stub are varied. Similar trade offs are observed in electroabsorption modulators [37].

For a specific modulation depth, the side-coupled-cavity switch results in more compact designs, when compared with the direct-coupled-cavity switch. For example, a side-coupled-cavity structure (Fig. 2(a)) with $w$ = 50nm, $L$ = 120nm achieves a modulation depth of ~20dB when varying the imaginary part of the refractive index from $\kappa = 0$ to $\kappa = 1$ (Fig. 3(a)). In the case of the direct-coupled-cavity structure (Fig. 1(a)), the same modulation depth is achieved for cavity length $L$ of ~430nm (Fig. 1(d)), i.e. the required cavity size is larger by a factor of ~3.6. We also found that for lower modulation depths, corresponding to lower pumping power densities and lower $\kappa$, the reduction in cavity size achieved by the side-coupled-cavity switch is even more dramatic. We note that the reduction of the required active material volume achieved by the side-coupled-cavity structure also results in reduction of the required pumping power.

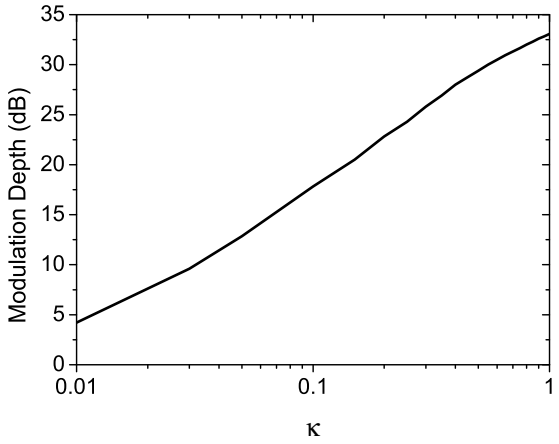


Fig. 5. Modulation depth $T(\kappa)/T(\kappa = 0)$ of the side-coupled-cavity switch (Fig. 2(a)) as a function of the imaginary part $\kappa$ of the refractive index. Results are shown for $w$ = 300nm, $L$ = 210nm. All other parameters are as in Fig. 2(b).

In Fig. 5, we show the modulation depth $T(\kappa)/T(\kappa = 0)$ of the side-coupled-cavity switch as a function of the imaginary part $\kappa$ of the refractive index. As expected, the modulation depth increases with $\kappa$. We also observe that even for a relatively small variation in the absorption coefficient of the material filling the cavity ($\Delta\kappa = 0.01$) we can achieve a modulation depth of ~60% (~4 dB). We note that such modulation depths have been demonstrated experimentally in other plasmonic absorption switches [15,17]. For a modulation depth of 99%, the required variation is $\Delta\kappa = 0.15$.

The side-coupled-cavity switch (Fig. 2(a)) was optimized at a single wavelength of $\lambda_0$ = 1.55μm. In Fig. 6 we show the modulation depth of the switch as a function of wavelength. We observe that there is a large wavelength range in which large modulation depth is achieved, i.e. the operation wavelength range of the switch is broad. More specifically, there is a ~30nm wavelength range in which the modulation depth is within 3dB of its maximum value. In comparison, in silicon modulators based on high-Q microring resonators the corresponding wavelength range is typically less than 1nm [38]. The broadband response of the device is due to the low quality factor $Q$ of the resonator associated, as mentioned above, with the low reflectivity at the waveguide-cavity interface.

#111340 - $15.00 USD Received 13 May 2009; revised 7 Jun 2009; accepted 8 Jun 2009; published 11 Jun 2009

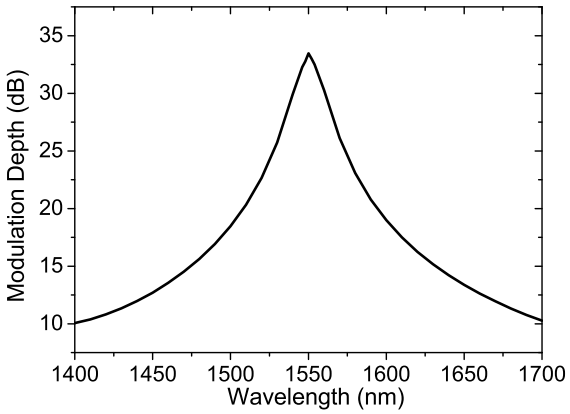


Fig. 6. Modulation depth $T(\kappa = 1)/T(\kappa = 0)$ of the side-coupled-cavity switch (Fig. 2(a)) as a function of wavelength. All other parameters are as in Fig. 5.

## 3. Conclusions

In this paper we first considered a switch consisting of a MDM plasmonic waveguide directly coupled to a cavity filled with an active material whose absorption coefficient can be modified with an external control beam. We found that such a direct-coupled-cavity structure can act as an absorption switch, in which the on/off states correspond to the absence/presence of pumping. The modulation depth of the switch increases almost exponentially with the cavity length.

We next considered a switch consisting of a MDM plasmonic waveguide side-coupled to a cavity filled with an active material. We found that the side-coupled structure can also operate as an absorption switch for MDM plasmonic waveguides, in which the on/off states correspond to the presence/absence of optical pumping. The modulation depth of the switch exhibits peaks when the cavity length is equal to one of the resonant lengths, and the maximum modulation depth is achieved at the first resonant length. We also found that the modulation depth is maximized for a specific cavity width. Variations in the imaginary part of the refractive index of the material filling the cavity of $\Delta\kappa = 0.01$ ($\Delta\kappa = 0.15$) result in ~60% (~99%) modulation depth. In addition, for the side-coupled-cavity switch there is a trade off between modulation depth and insertion loss, as the geometrical parameters of the stub are varied. Finally, the operation wavelength range of the switch is broad.

We found that for a specific modulation depth, the side-coupled-cavity switch results in more compact designs, when compared with the direct-coupled-cavity switch. The reduction in required cavity size and pumping power achieved by the side-coupled-cavity switch is more dramatic for lower modulation depths. The properties of both switches can be accurately described using the concept of characteristic impedance and transmission line theory.

As final remarks, for the active material considered in this paper (QD-doped silicon dioxide), the switching time of the absorption switches is limited by the QD-exciton recombination lifetime which is on the order of 40 ns [16,17]. In addition, we estimate that the pumping power of the switches will be on the order of 100nW, by considering the cavity area and the required pumping power density [16,17]. Such low power operation is enabled by the high QD absorption cross section [16,17], and the nanoscale size of the device. We also note that, in addition to the active material considered in this paper, a variety of other materials with tunable absorption coefficient can be used. These include multiple quantum well structures typically used in electroabsorption modulators [39], heavily-doped silicon [40], and photochromic molecules [15]. The use of heavily-doped silicon could lead to switching times of less than 1 ps [40].

#111340 - $15.00 USD Received 13 May 2009; revised 7 Jun 2009; accepted 8 Jun 2009; published 11 Jun 2009